ISSN 1063-7826, Semiconductors, 2017, Vol. 51, No. 3, pp. 310–317. © Pleiades Publishing, Ltd., 2017.
Original Russian Text © G.B. Galiev, M.M. Grekhov, G.Kh. Kitaeva, E.A. Klimov, A.N. Klochkov, O.S. Kolentsova, V.V. Kornienko, K.A. Kuznetsov, P.P. Maltsev, S.S. Pushkarev, 2017, published in Fizika i Tekhnika Poluprovodnikov, 2017, Vol. 51, No. 3, pp. 322–330.

SPECTROSCOPY, INTERACTION WITH RADIATION

Terahertz-Radiation Generation in Low-Temperature InGaAs Epitaxial Films on (100) and (411) InP Substrates

G. B. Galiev[a]*, M. M. Grekhov[c], G. Kh. Kitaeva[b], E. A. Klimov[a], A. N. Klochkov[a], O. S. Kolentsova[c], V. V. Kornienko[b], K. A. Kuznetsov[b], P. P. Maltsev[a], and S. S. Pushkarev[a]

[a] *Institute of Ultra-High Frequency Semiconductor Electronics, Russian Academy of Sciences, Moscow, 117105 Russia*

[b] *Moscow State University, Faculty of Physics, Moscow, 119991 Russia*

[c] *National Research Nuclear University "MEPhI", Moscow, 115409 Russia*

**e-mail: galiev_galib@mail.ru*

Submitted May 10, 2016; accepted for publication May 18, 2016

Abstract—The spectrum and waveforms of broadband terahertz-radiation pulses generated by low-temperature $In_{0.53}Ga_{0.47}As$ epitaxial films under femtosecond laser pumping are investigated by terahertz time-resolved spectroscopy. The $In_{0.53}Ga_{0.47}As$ films are fabricated by molecular-beam epitaxy at a temperature of 200°C under different arsenic pressures on (100)-oriented InP substrates and, for the first time, on (411)A InP substrates. The surface morphology of the samples is studied by atomic-force microscopy and the structural quality is established by high-resolution X-ray diffraction analysis. It is found that the amplitude of terahertz radiation from the LT-InGaAs layers on the (411)A InP substrates exceeds that from similar layers formed on the (100) InP substrates by a factor of 3–5.

DOI: 10.1134/S1063782617030071

1. INTRODUCTION

In recent years, photoconductive antennas for transmitting and receiving terahertz (100 GHz to 10 THz) electromagnetic signals on the basis of III–V epitaxial compounds grown at low temperatures have been objects of intense study. One of the first compounds used for this purpose was GaAs grown at low-temperatures (LT-GaAs), which is characterized by an ultrashort lifetime of photoexcited charge carriers, high dark resistivity, and high electron mobility [1]. Many available devices are designed on the basis of LT-GaAs [2].

Low-temperature growth leads to the incorporation of excess As atoms into the LT-GaAs crystal lattice and to the formation of defects, including arsenic atoms at gallium atomic sites As_{Ga} (antisite defects), As_i interstitials, and gallium vacancies V_{Ga}.

The trapping of photoexcited electrons and their short lifetime are determined mainly by As_{Ga} defects [3]. However, to trap an electron, the As_{Ga} defect should be in the charged state As_{Ga}^{+}; i.e., the arsenic atom should lose the fifth external electron. To enhance the concentration of charged As_{Ga}^{+} defects, the LT-InGaAs material is doped with an acceptor impurity, most frequently with beryllium [4]. As was shown in [3, 5, 6], under certain doping concentrations (from 5×10^{17} to 2×10^{19} cm^{-3}), Be:LT-GaAs structures are obtained which can be used in terahertz optoelectronic devices. The parameters of such devices are better than those of undoped LT-GaAs-based ones. However, the high toxicity of beryllium requires additional safety measures for its use in molecular-beam epitaxy (MBE). In addition, the presence of a Be source in a MBE facility enhances the background p-type impurity concentration, which negatively affects other heterostructures grown in the facility.

It was demonstrated [7–12] that the amphoterism of silicon atoms in GaAs with the (n11)A orientation, where $n = 1, 2, 3, \ldots$, during high-temperature MBE growth allows epitaxial films with both n- and p-type conductivity to be obtained. The conductivity type depends on the arsenic pressure during MBE growth. Based on these results, we fabricated a planar p–n junction by MBE growth on the (111)A GaAs substrates with the use of only a silicon dopant [13, 14]. As far as we know, there have been no studies on the effect of polar (n11)A substrate orientation on the type of conductivity of Si-doped GaAs films epitaxially grown at low temperatures, as well as studies on similar effects in InGaAs films on InP substrates. Recently, we presented for the first time the results of investigations of the structural and photoluminescent properties of LT-GaAs structures on GaAs (111)A and (100) substrates [15, 16].

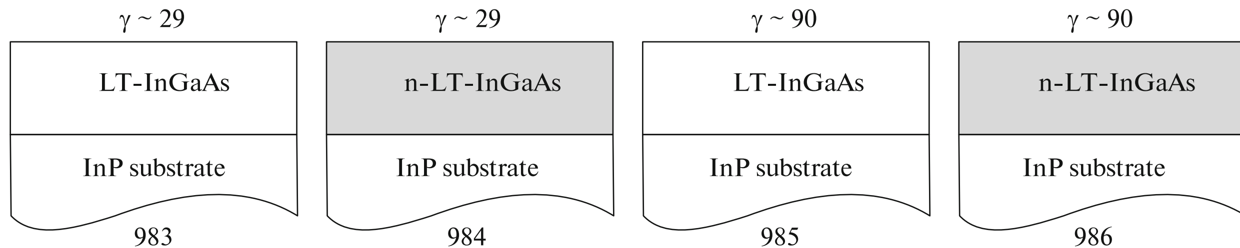

Fig. 1. Sample design, $\gamma = P_{As}/(P_{Ga} + P_{In})$.

One of the factors narrowing the range of application of the LT-InGaAs-based photoconductive antennas is the wide band gap of GaAs (E_g = 1.424 eV, the pump wavelength $\lambda \leq 871$ nm). This limits the choice of femtosecond laser sources that can operate with such antennas. In view of this, it is important to develop materials compatible with the available low-cost lasers used in fiber-optic communication (1.3 and 1.55 μm), which would simultaneously have all the above-mentioned advantages.

One suitable material is InGaAs with a narrow band gap (the band gap of $In_{0.53}Ga_{0.47}As$ is E_g = 0.718 eV, the pump wavelength is $\lambda \leq 1.727$ nm [17]). However, even undoped LT-InGaAs epitaxial layers have a high conduction electron density (~10^{17} cm^{-2}) and low dark resistivity. Therefore, one of the fundamental problems in this field is the development of InGaAs film fabrication conditions that would ensure the film parameters required for photoconductive terahertz antennas, i.e., the short photoexcited-carrier lifetime and the maximum possible dark resistivity.

Studies in this field are focused on the following items:

(i) Ion bombardment of InGaAs films with high-energy ions [18, 19].

(ii) Doping of the InGaAs layer with Be acceptors during low-temperature epitaxy [20, 21] or with impurities forming deep levels (Fe) [22].

(iii) Formation of periodical nanoscale ErAs islands with thicknesses of 0.2–2 monolayers in the LT-InGaAs epitaxial films [23–25].

This study is devoted to the following. The use of InP substrates with the (n11)A orientation, where n = 1, 2, 3, ..., makes it possible, as in the case of (111)A GaAs substrates, to technologically control the deposition of silicon atoms at lattice sites of Group-III or -V elements, which make the latter either donors or acceptors of electrons. Incorporation is controlled during MBE by changing the arsenic pressure or dopant concentration. Thus, the LT-InGaAs resistivity and concentration of electron traps coupled with antisite defects can be increased.

2. EXPERIMENTAL

The samples under study were grown on Fe-doped semi-insulating InP substrates by MBE. The design of the samples is illustrated in Fig. 1. The samples are 1.2-μm-thick LT-$In_{0.53}Ga_{0.47}As$ layers on InP substrates of two types: with the (100) and (411)A crystallographic orientations. The grown samples were either undoped or homogeneously doped with silicon. When growing the doped samples (984 and 986), the silicon-cell temperature was 1040°C, which corresponds to a bulk electron concentration of (4–5) × 10^{17} cm^{-3} at the high-temperature growth of n-GaAs on the GaAs (100) substrate.

To obtain the maximum identity of the technological conditions (growth temperature T_g and ratio γ between the Group-V and -III element flows), two halves of different substrates were mounted on a sample holder in one process. Samples 983 and 984 were grown at γ ~ 29 and samples 985 and 986, at γ ~ 90. The temperature of LT-InGaAs layer growth was the same for all the samples and amounted to 200°C. The grown samples were annealed in the growth chamber of the MBE facility in the As_4 flow at a temperature of 500°C for 1 h. Hereinafter, the samples on the (100) InP substrates are referred to as 983-O, 984-O, 985-O, and 986-O and the samples on the (411)A InP substrates, are referred to as 983-A, 984-A, 985-A, and 986-A.

The surface morphology of the samples was studied by atomic-force microscopy (AFM) using a Solver Next (NT MDT) microscope and the diffraction reflection curves (DRCs) were measured using a Rigaku Ultima IV diffractometer.

The generation of terahertz electromagnetic radiation in the LT-InGaAs layers was studied in samples subjected to high-temperature annealing. A schematic representation of the terahertz time-resolved spectroscopy (TTRS) facility is shown in Fig. 2. The optical-radiation-pulse source was a femtosecond Er^{3+} fiber laser with a wavelength of 1.56 μm, a pulse length of 100 fs, and a pulse-repetition rate of 70 MHz. After passing a focusing lens and a beam splitter, a part of the radiation with an average power of 20 mW was brought to the terahertz photoconductive detecting antenna through a system of mirrors in order to create

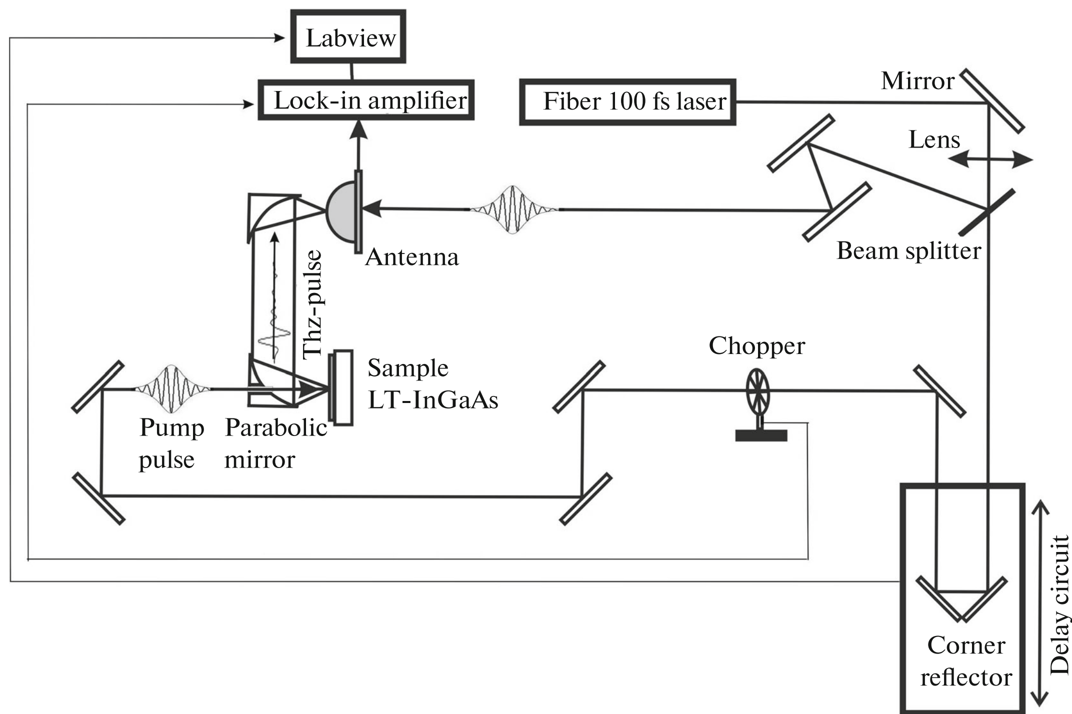

Fig. 2. Schematic of the TTRS setup.

free charge carriers in the antenna heterostructure. The fundamental beam with a power of 100 mW was directed to a controlled delay line, then to a mechanical beam modulator rotating with a frequency of 2.3 kHz, and, finally, to the investigated sample through an aperture in a parabolic mirror. The terahertz radiation generated in the sample was collected by a pair of parabolic mirrors and focused on a silicon lens integrated with the terahertz antenna. The antenna free-charge-carrier current modulated by terahertz radiation was detected with a synchronous detector. Thus, the strength of the field of terahertz waves generated in the direction opposite to pumping was measured at different instants of time after the arrival of a pump pulse. All the units of the facility were controlled using Labview software.

3. AFM STUDY OF THE SAMPLES

Figure 3 shows AFM images of the surface of the samples under study. It can be seen that the surface morphology of the samples depends on the γ value at which they were grown. The dependence on γ is stronger for the samples grown on the (100) InP substrates. At $\gamma \sim 29$, separate pits are observed on a relatively smooth surface (sample 983-O). An increase in the γ value to 90 leads to the formation of a more complex granular surface pattern, in which small (0.2–0.3 μm) grains are grouped into larger (0.8–1.6 μm) irregular agglomerates (sample 985-O).

The surface of the samples on the InP (411)A substrates at $\gamma \sim 29$ is fine-grained with a grain size of 0.2–0.3 μm. As in the samples on InP (100), an increase in the γ value to 90 results in a large-scale pattern with an agglomerate size of 0.8–1.6 μm (sample 985-A). The measured root-mean-square roughness (R_q) values are given in Table 1. According to these data, annealing of the samples on the InP (411)A substrates leads to a larger increase in R_q than in the samples on InP (100). The surface pattern morphology does not fundamentally change after annealing.

The observed regularities in the variation of the LT-InGaAs film surface morphology with the As_4 flow intensity (the smoother surface corresponds to a weak As_4 flow and the rough surface corresponds to a strong one) are consistent with the data from [26]

Table 1. Root-mean-square roughness of the LT-InGaAs sample surface

Substrate orientation		(100)		(411)A	
Sample		983-O	985-O	983-A	985-A
γ		29	90	29	90
R_q, nm	Before annealing	3.9	15.9	5.7	7.3
	After annealing	3.7	16.3	9.0	14.3

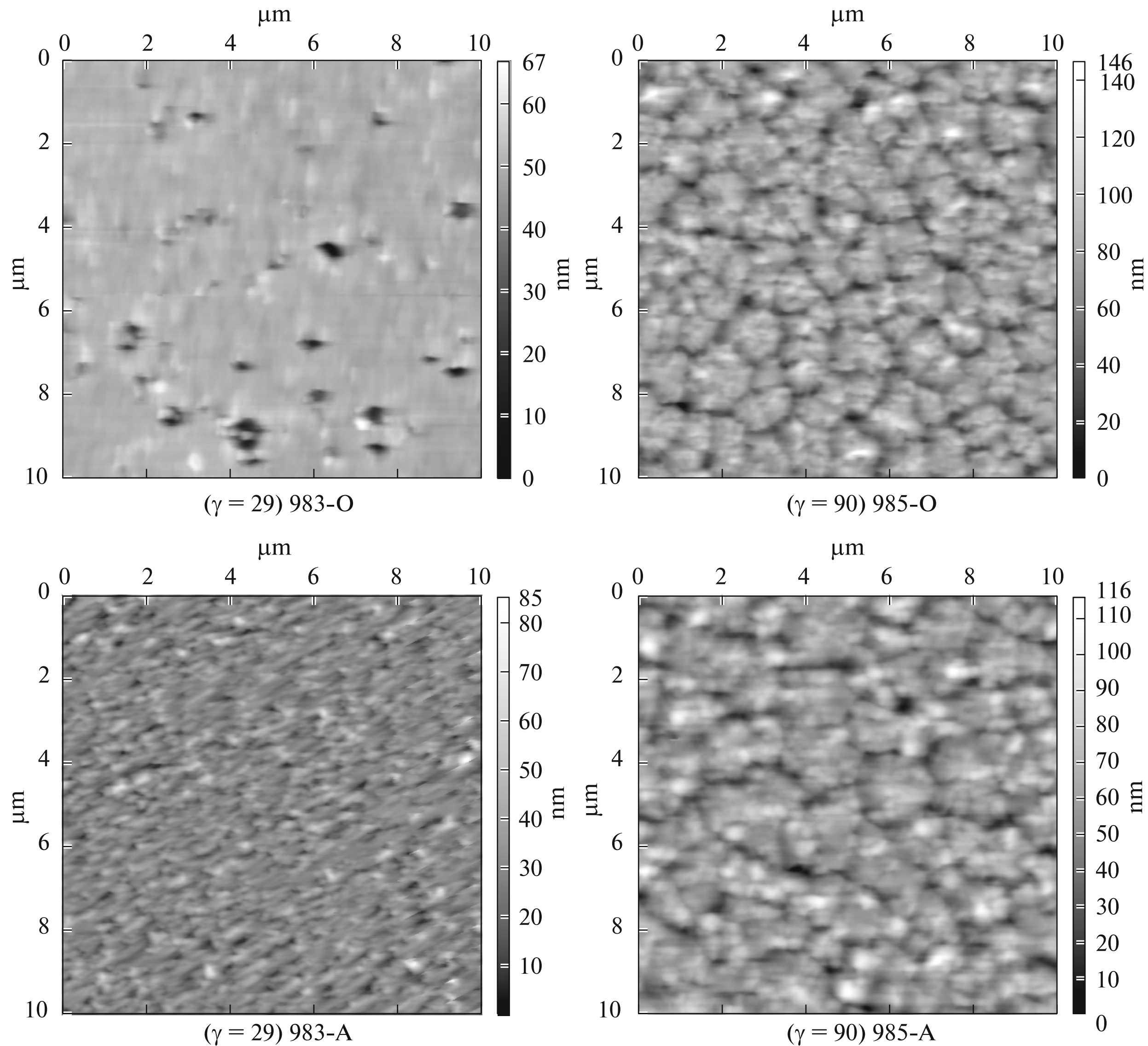

Fig. 3. AFM images of annealed samples.

related to the corresponding LT-InGaAs growth temperature (200°C).

4. HIGH-RESOLUTION X-RAY DIFFRACTOMETRY OF THE SAMPLES

In the crystals with the zinc-blende structure, including InGaAs and InP, X-ray diffraction reflection from the (411) planes does not occur, since the condition of the same parity of indices is violated [27]. Therefore, in studying the samples on the (411) A InP substrates, we observed reflection from the (311) planes at a small angle of incidence of the X-ray beam.

Figure 4 shows DRCs for the investigated samples before and after annealing. The common feature of all the curves is an intense narrow peak *1* corresponding to the InP substrate. The difference between the DRCs for the samples grown on the (100) and (411)A InP substrates consists in the following: the DRCs of the samples on (100) InP include an additional peak (peak *2*) with a much lower intensity and larger width than peak *1*. This additional peak can be located both on the left (samples 983-O and 984-O) and on the right (samples 985-O and 986-O) from the fundamental peak in angular coordinates. After annealing, peak *2* for sample 983-O changes its position relative to the substrate peak and shifts to larger angles. This is indicative of a decrease in the LT-InGaAs lattice parameter after annealing. This behavior of peak *2* is observed only for samples 983 and 984. The specificity of these samples is that the LT-InGaAs layer in sample 984 was uniformly doped with silicon at a concentration of $N_{Si} = 5 \times 10^{17}$ cm^{-3}. Under our experimental

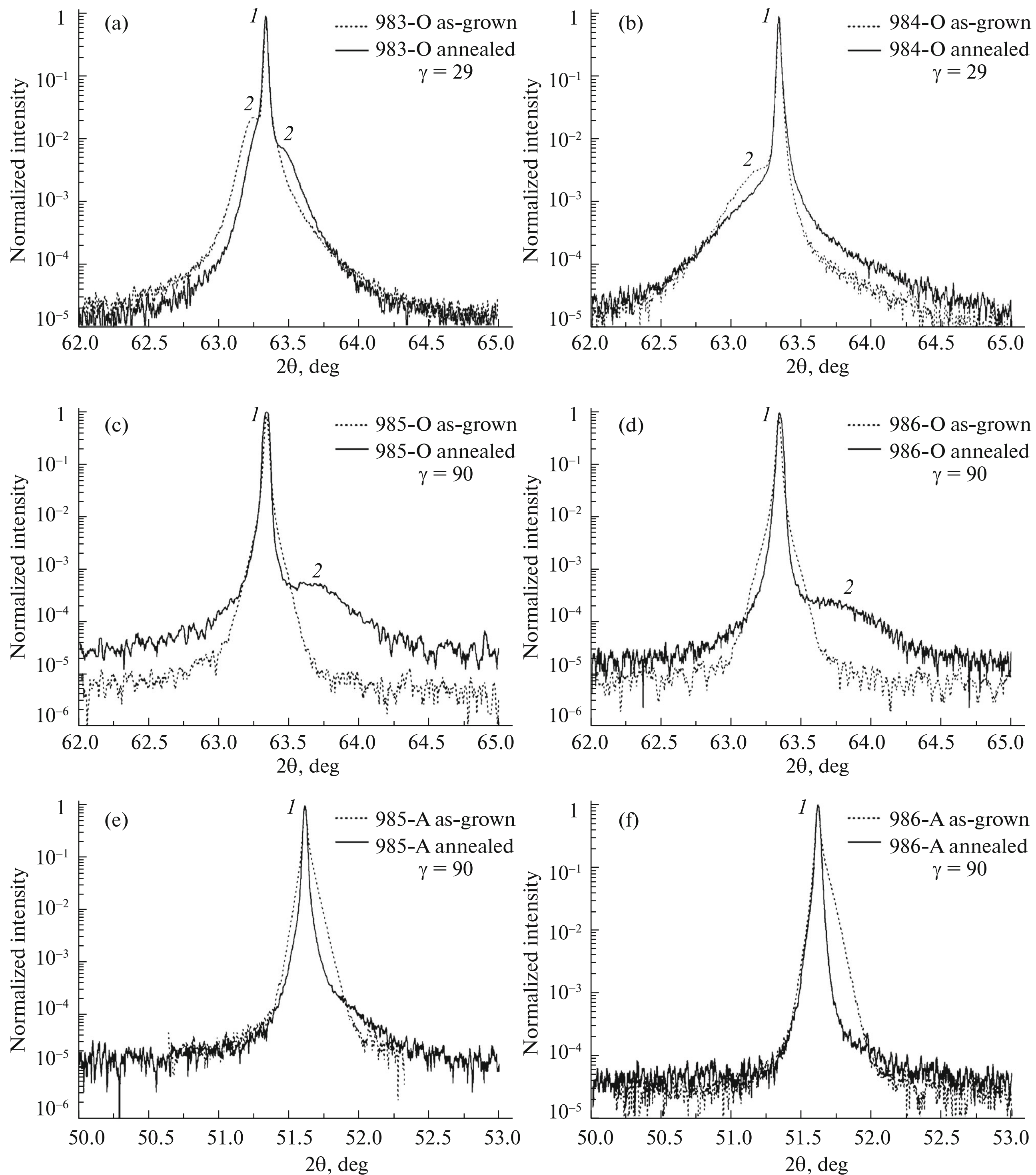

Fig. 4. DRCs of the investigated samples in the θ/2θ scanning mode. (a–d) Samples on InP (100) substrates, (400) reflection and (e, f) samples on the InP (411)A substrates, (311) reflection.

conditions, the Si-cell temperature was 1040°C. In our opinion, the different behavior of peak *2* for samples 983-O and 984-O upon annealing is related to the additional annealing of sample 984-O during LT-InGaAs epitaxial growth due to radiation-induced heating by the Si atom source, as in study [28], where Missous reported the effect of heated dopant (Si and Be) sources on the amount of excess arsenic in the LT-InGaAs lattice, which, in turn, affects the DRC shape.

Table 2. Lattice parameters of the LT-InGaAs layers

Sample		983-O	984-O	985-O	985-A	986-O	986-A
a, Å	Unannealed	5.877 ± 0.001	5.887 ± 0.005	–*	–	–	–
	Annealed	5.856 ± 0.002	–	5.853 ± 0.007	–	5.832 ± 0.007	–

*"–" signifies the absence of a peak in the DRCs

In contrast to the DRCs of the samples on the (100) InP substrates, the DRCs of the samples on the (411)A InP substrates do not contain a noticeable peak *2*; at the same time, after annealing peak *1* narrows and acquires a small asymmetric shoulder on the right. This can be indicative of the initial coincidence of the lattice parameters of the InP substrate and LT-InGaAs film, due to which peak *2* is masked by peak *1*, as well as an increase in the LT-InGaAs lattice parameter after annealing.

The lattice parameters of the LT-InGaAs layer calculated from the angular position of peak *2* are given in Table 2.

5. TERAHERTZ TIME-RESOLVED SPECTROSCOPY OF THE SAMPLES

Figures 5a and 5b show the measured time dependences of the strength of the electromagnetic field induced in all the investigated LT-InGaAs samples. After the interband absorption of pump radiation pulses, photoexcited electrons and holes formed a rapidly changing electric current under the action of the electric field. Current spikes led to the generation of electromagnetic pulses. Since the investigated samples had no ohmic contacts and were not biased, photoexcited carriers moved under the action of a built-in electric field (surface potential) or by means of different diffusion lengths of electrons and holes (Dember effect). In all the cases, the waveforms of the detected signals consist of two pulses with approximately the same shape and amplitude; the pulses are separated in time. The second pulse observed ~10 ps after the first pulse is not related to the reflection of a terahertz wave from the InP substrate, since the absorption coefficient of indium phosphide reaches about 100 cm^{-1} in this frequency range [29] and the observed second signal has an amplitude no smaller than that of the first signal. The TTRS measurements on the "empty" (100) InP and (411)A InP substrates showed that generation in them is lacking or is weaker by one–two orders of magnitude. Thus, the observed terahertz-radiation signals are generated in micrometer-thick LT-InGaAs layers. According to the estimation, the second pulse is related to laser pump re-reflection from the backside of the InP substrate with a thickness of 400 μm with subsequent terahertz-radiation generation in a micrometer-thick LT-InGaAs layer in the forward geometry. Taking into account the weak absorption of the laser pump in the substrate material and the loss upon pump reflection from the dull sample backside, we can conclude that the generation efficiency in the pump direction should be somewhat higher than in the opposite direction.

Table 3. Maximum values of the induced field strength (arb. units)

Substrate orientation	Sample				
	983	984	985	986	InP
(100)	0.07	0.05	0.06	0.06	0.01
(411)A	0.17	0.10	0.19	0.07	0.02

It can be seen from Fig. 5 that in all the samples grown on the (411)A InP substrates the amplitude of generated waves is approximately twice as large as in the samples on (100) InP. For comparison, Table 3 gives the maximum strengths of the electric field detected for different samples (in the same relative units).

The spectral composition of the generated pulses was determined using the Fourier transform of time domains. The obtained normalized frequency distributions of the spectral amplitudes of signals from samples 985 and 986 did not depend, within good accuracy, on the substrate orientation. However, it was found that the spectral forms of the radiation from samples 983 and 984 depend significantly on the substrate type. Comparison of Figs. 5a and 5b shows that the samples grown on the (411)A InP substrates generate more intense high-frequency radiation than the samples on (100) InP. We can conclude that, in the LT-InGaAs epitaxial films grown on the (411)A InP substrates, the concentration of As_{Ga}^{+} traps is enhanced or traps are formed that are related to other point defects, which trap electrons more efficiently.

The use of a higher As_4 pressure during LT-InGaAs film growth ($\gamma \sim 90$ instead of 29) led to a change in the time dependence of the pulse, which affected the spectral composition of the radiation. Figure 6 shows the spectral dependences of the intensity of radiation generated in samples 983-A and 985-A on the (411)A InP substrates. In the calculation, we took into account the frequency response of the detecting antenna. The detected radiation-generation spectra of the samples are located in the range of 50–600 GHz. At frequencies below 50 GHz, the sensitivity of the photoconductive antenna decreases by more than an order of magnitude; therefore, we cannot draw an

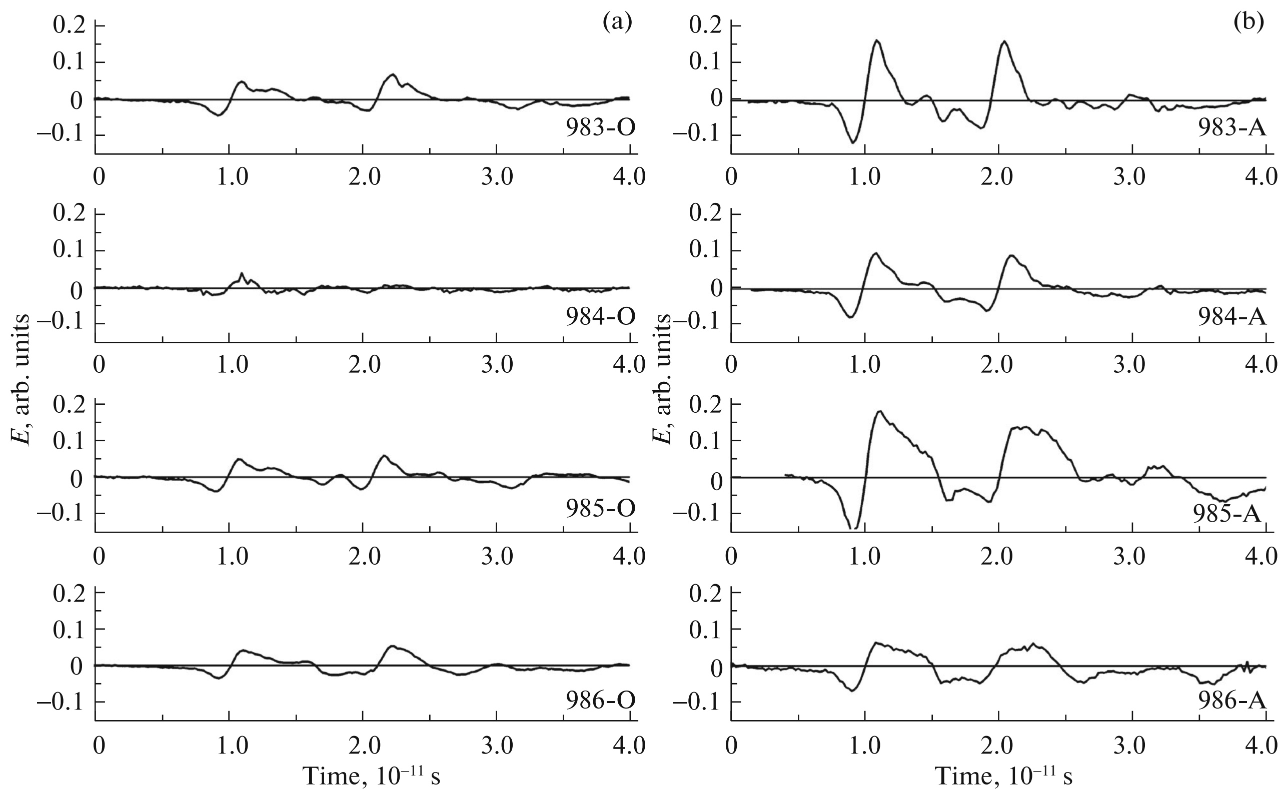

Fig. 5. Dependences of the strength of the electromagnetic field induced by the LT-InGaAs layers on the time after arrival of the laser pump pulse. (a) Samples on the InP (100) substrates and (b) samples on the InP (411)A substrates.

exact conclusion about the spectral response of the samples in this range. In the samples grown under a high As_4 pressure, the maximum in the radiation spectrum is slightly shifted to the low-frequency region and has a twice as large amplitude as the maximum in the generation spectrum of the samples grown at a low As_4 pressure. This indicates a higher generation efficiency at frequencies below 200 GHz in the samples with a larger number of electron traps at defects.

Doping of the LT-InGaAs layers with Si atoms led to an approximately twofold decrease in the amplitude of the terahertz-radiation strength (a decrease in the intensity by a factor of about four) for both substrate types and both As_4 pressures used. The time dependence of radiation pulses and the spectral composition of the radiation did not depend on the presence of Si impurity in the LT-InGaAs layers. This can be attributed to the fact that, as we mentioned in the Introduction, the As_{Ga} antisite defects operate as electron traps only in the electron-free charged state As_{Ga}^{+}. When the substance is doped with the Si donor impurity, electrons from the Si levels pass to the As_{Ga} levels and fill them. Consequently, the concentration of active As_{Ga}^{+} traps decreases, the photoexcited carrier current changes in time to a slighter extent, and the terahertz-radiation intensity drops.

Thus, the presented data show that the (n11)A InP substrates can turn out to be preferable for application in terahertz-radiation sources. Use of the other above-mentioned manipulations with LT-InGaAs layers can improve the qualitative and quantitative characteristics of devices based on LT-InGaAs structures with the (n11)A orientations as compared with the case of the (100) orientation.

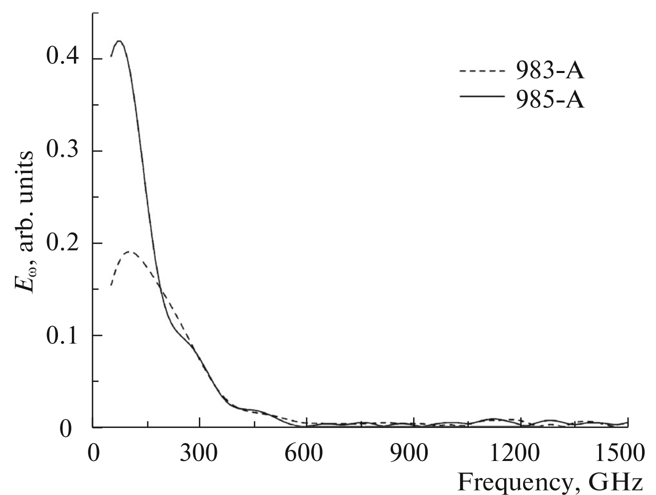

Fig. 6. Spectrum of pulses generated in samples 983-A and 985-A on the InP (411)A substrates.

6. CONCLUSIONS

The LT-$In_{0.53}Ga_{0.47}As$ films grown at a low As_4 pressure (γ = 29) have a moderately rough surface (R_q = 4–9 nm) and, with increasing As_4 pressure (γ = 90), the surface roughness of the films significantly increases (R_q = 14–16 nm). The use of InP substrates with the (411)A orientation somewhat increases the surface roughness of the samples grown at the same γ value. It is established that the structural quality of the LT-InGaAs films is affected by the As_4 pressure to a greater extent than by the substrate orientation.

Under irradiation of the investigated samples by femtosecond pulses of an IR Er^{3+} fiber laser, radiation in the frequency band up to 300 GHz with a maximum at ~70–100 GHz is generated.

It is observed that the efficiency of terahertz-radiation generation by the LT-InGaAs films on InP substrates with the (411)A crystallographic orientation of the surface exceeds the value for the same films on the (100) InP substrates by a factor of three–five.

The use of a higher As_4 pressure during LT-InGaAs film growth (γ ~ 90 instead of 29) leads to a change in the time shape of the terahertz pulse, which affects the terahertz-radiation spectrum: its maximum shifts toward lower frequencies. In this case, the integral terahertz-radiation intensity increases.

Doping of the LT-InGaAs films with Si atoms leads to an approximately twofold decrease in the terahertz-radiation amplitude (a decrease in the intensity by a factor of ~ 4); the time shape and spectral composition of radiation pulses do not change.

ACKNOWLEDGMENTS

We thank Candidate of Physical and Mathematical Sciences D.V. Lopaev for his help in the experiments.

This study was supported by the Russian Foundation for Basic Research (project nos.16-02-00258, 16-29-03294, 16-32-00693, and 16-07-00187 A) and the Grant of the President of the Russian Federation SP-686.2016.3.

REFERENCES

1. E. A. P. Prieto, S. A. B. Vizcara, A. S. Somintac, A. A. Salvador, E. S. Estacio, C. T. Que, K. Yamamoto, and M. Tani, J. Opt. Soc. Am. B **31**, 291 (2014).
2. A. Krotkus, J. Phys. D: Appl. Phys. **43**, 273001 (2010).
3. A. Krotkus, K. Bertulis, L. Dapkus, U. Olin, and S. Marcinkevičius, Appl. Phys. Lett. **75**, 3336 (1999).
4. Toshihiko Ouchi and Kousuke Kajiki, US Patent No. 8835853 (2014).
5. J.-L. Coutaz, J.-F. Roux, A. Gaarder, S. Marcinkevicius, J. Jasinski, K. Korona, M. Kaminska, K. Bertulis, and A. Krotkus, in *Proceedings of the 11th International Semiconducting and Insulating Material Conference, Canberra, Australia, July 3–7, 2000,* p. 89.
6. P. Specht, S. Jeong, H. Sohn, M. Luysberg, A. Prasad, J. Gebauer, R. Krause-Rehberg, and E. R. Weber, Mater. Sci. Forum **258–263**, 251 (1997).
7. J. Maguire, R. Murray, R. C. Newman, R. B. Beall, and J. J. Harris, Appl. Phys. Lett. **50**, 516 (1987).
8. E. F. Schubert, J. E. Cunningham, and W. T. Tsang, Solid State Commun. **63**, 591 (1987).
9. Y. Okano, H. Seto, H. Katahama, S. Nishine, I. Fujimoto, and T. Suzuki, Jpn. J. Appl. Phys. **28**, L151 (1989).
10. F. Piazza, L. Pavesi, M. Henini, and D. Johnston, Semicond. Sci. Technol. **7**, 1504 (1992).
11. L. Pavesi, F. Piazza, M. Henini, and I. Harrison, Semicond. Sci. Technol. **8**, 167 (1993).
12. M. Henini, N. Galbiati, E. Grilli, M. Guzzi, and L. Pavesi, J. Cryst. Growth **175–176**, 1108 (1997).
13. G. B. Galiev, V. E. Kaminski, V. G. Mokerov, and L. E. Velikhovski, Semiconductors **35**, 415 (2001).
14. G. B. Galiev, V. Kaminskii, D. Milovzorov, L. Velihovskii, and V. G. Mokerov, Semicond. Sci. Technol. **17**, 120 (2002).
15. G. B. Galiev, E. A. Klimov, M. M. Grekhov, S. S. Pushkarev, D. V. Lavrukhin, and P. P. Maltsev, Semiconductors **50**, 195 (2016).
16. D. V. Lavrukhin, A. E. Yachmenev, A. S. Bugaev, G. B. Galiev, E. A. Klimov, R. A. Khabibullin, D. S. Ponomarev, and P. P. Maltsev, Semiconductors **49**, 911 (2015).
17. S. Adashi, *Properties of Semiconductor Alloys: Group-IV, III–V and II–VI Semiconductors* (Wiley, New York, 2009).
18. J. Mangeney, F. Meng, D. Gacemi, E. Peytavit, J. F. Lampin, and T. Akalin, Appl. Phys. Lett. **97**, 161109 (2010).
19. J. Mangeney, N. Chimot, L. Meignien, N. Zerounian, P. Crozat, K. Blary, J. F. Lampin, and P. Mounaix, Opt. Express **15**, 8943 (2007).
20. B. Sartorius, H. Roehle, H. Kunzell, J. Böttcher, M. Schlak, D. Stanze, H. Venghaus, and M. Schell, Opt. Express **16**, 9565 (2008).
21. A. Takazato, M. Kamakura, T. Matsui, J. Kitagawa, and Y. Kadoya, Appl. Phys. Lett. **91**, 011102 (2007).
22. C. D. Wood, O. Hatem, J. E. Cunningham, E. H. Linfield, A. G. Davies, P. J. Cannard, M. J. Robertson, and D. G. Moodie, Appl. Phys. Lett. **96**, 194104 (2010).
23. F. Ospald, D. Maryenko, K. von Klitzing, D. C. Driscoll, M. P. Hanson, H. Lu, A. C. Gossard, and J. H. Smet, Appl. Phys. Lett. **92**, 131117 (2008).
24. M. Sukhotin, E. R. Brown, D. Driscoll, M. Hanson, and A. C. Gossard, Appl. Phys. Lett. **83**, 3921 (2003).
25. D. C. Driscoll, M. Hanson, C. Kadow, and A. C. Gossard, Appl. Phys. Lett. **78**, 1703 (2001).
26. M. D. Vilisova, I. V. Ivonin, L. G. Lavrent'eva, S. V. Subach, M. P. Yakubenya, V. V. Preobrazhenskii, M. A. Putyato, B. R. Semyagin, N. A. Bert, Yu. G. Musikhin, and V. V. Chaldyshev, Semiconductors **33**, 824 (1999).
27. B. K. Vainshtein, *Modern Crystallography* (Nauka, Moscow, 1979), Vol. 1 [in Russian].
28. M. Missous, Microelectron. J. **27**, 393 (1996).
29. C. Zhang, B. Jin, J. Chen, P. Wu, and M. Tonouchi, J. Opt. Soc. Am. B **26** (9), A1 (2009).

Translated by E. Bondareva